

Review

Hydrotalcite-Type Materials Electrodeposited on Open-Cell Metallic Foams as Structured Catalysts

Phuoc Hoang Ho, Erika Scavetta, Domenica Tonelli, Giuseppe Fornasari, Angelo Vaccari 
and Patricia Benito * 

Dipartimento di Chimica Industriale “Toso Montanari”, Università di Bologna,
Viale Risorgimento 4, 40136 Bologna, Italy; hoangphuocho@gmail.com (P.H.H.); erika.scavetta2@unibo.it (E.S.);
domenica.tonelli@unibo.it (D.T.); giuseppe.fornasari@unibo.it (G.F.); angelo.vaccari@unibo.it (A.V.)

* Correspondence: patricia.benito3@unibo.it; Tel.: +39-051-2093643

Received: 10 June 2018; Accepted: 26 July 2018; Published: 29 July 2018



Abstract: Structured catalysts based on hydrotalcite-derived coatings on open-cell metallic foams combine tailored basic/acidic sites, relatively high specific surface area and/or metal dispersion of the coating as well as low pressure drop and enhanced heat and mass transfer of the 3D metallic support. The properties of the resulting structured catalysts depend on the coating procedure. We have proposed the electro-base generation method for in situ and fast precipitation of Ni/Al and Rh/Mg/Al hydrotalcite-type materials on FeCrAlloy foams, which after calcination at high temperature give rise to structured catalysts for syngas (CO + H₂) production through Steam Reforming and Catalytic Partial Oxidation of CH₄. The fundamental understanding of the electrochemical-chemical reactions relevant for the electrodeposition and the influence of electrosynthesis parameters on the properties of the as-deposited coatings as well the resulting structured catalysts and, hence, on their catalytic performance, were summarized.

Keywords: electrodeposition; hydrotalcite-type compounds; nickel; rhodium; FeCrAlloy foam; structured catalyst; steam reforming; catalytic partial oxidation

1. Introduction

Open-cell metallic foams are promising supports to develop the so-called structured catalysts for process intensification [1,2]. The cellular foam structure made by interconnecting struts provides high geometrical surface area, low pressure drop, enhanced mass and heat transfer [3–6]. The performances of the structured catalysts depend not only on the properties of the deposited materials (loading, composition, size and dispersion of active species, textural characteristics), but also on the adhesion of the coating layer onto the surface of the foams. Metallic foams have been coated by the same procedures used to coat their honeycomb monoliths counterparts: (i) the deposition of catalyst slurries [7–10]; (ii) the deposition of catalyst supports followed by impregnation of the active phase [11–13]; and (iii) the in situ synthesis of the catalyst [14–17]. Washcoating may show some drawbacks such as the modification of the catalyst properties [9] or the pore blockage, indeed medium or large pore foams have been coated [18,19]. On the other hand, the synthesis and deposition of the catalytic species by hydrothermal treatment offers some advantages such as the absence of additives and binders, and the simpler and faster procedure [14,20,21]. However, the precipitation may simultaneously occur in the bulk solution leading to some loss of the active materials.

Electrochemical deposition is an easy route to coat in one-step, at room temperature, electrically conductive supports with metallic particles, hydroxides and oxides or a combination of them [22–32], which can be exploited for the preparation of structured catalysts. These electrochemical depositions can be performed by applying a cathodic potential in a continuous or pulsed mode to a working

electrode, which is the substrate that must be coated. For the deposition of metallic particles, the applied potential and the bath solution must be chosen so that the direct electrochemical reduction of the metal precursors occurs. On the contrary, in the deposition of hydroxides or oxides the electro-base generation method is applied. The basic medium at the electrode-electrolyte interface provokes the chemical precipitation of the cations in the solution directly on the electrode surface. The reduction of some electroactive species, e.g., dissolved oxygen, water, and nitrate consumes H^+ or generates OH^- , thus being responsible of the pH increase. The electrodeposition of hydroxides was originally developed for the modification of small and simple-shaped electrodes with $Ni(OH)_2$ [33,34] and it was later extended to the deposition of more complex hydrotalcite-type (HT) compounds, also called layered double hydroxides, with general formula $[M^{2+}_{1-x}M^{3+}_x(OH)_2](A^{n-})_{x/n} \cdot mH_2O$. Ni/Al [35] and Co/Al or Co/Cr HTs [36] were initially synthesized onto a Pt-foil cathode then Ni/Co, Ni/Fe, and Co/Fe formulations were applied as sensors [37], redox supercapacitors [38,39] and, more recently, as electrocatalysts, mainly for oxygen evolution reaction [40–42]. In these two latter fields, there is a growing interest in replacing conventional 2D by 3D supports such as fibers [43,44] and open-cell foams [45–47].

In this context, we reported for the first time in 2008 the electro-base generation method to coat FeCrAlloy foams with HT compounds for the preparation of H_2 production structured catalysts [48]. Later, electrodeposition has been used to coat FeCrAlloy foams by Rh [49], Pt [50] and Pt-CeO₂ [51], as gas-phase structured catalysts. The integration of HT compounds on metallic open-cell foams results in structured catalysts that take advantage of both the above commented properties of open-cell foams and the intrinsic properties of HT materials, e.g., high specific surface area and/or metal dispersion, basicity, thermal stability. Although cathodic electrodeposition of HT compounds has been investigated since the 1990s [35], the coating of complex-shaped foams with thick HT coatings for the preparation of precursors of catalysts was novel and not straightforward. Hence, several parameters had to be adjusted to demonstrate that it could be exploited for the preparation of structured catalysts in which the loading, and type of active components play an important role in the catalytic performances. Firstly, the coating layer must reach a certain thickness (e.g., 20 μm or thicker) to provide sufficient catalyst loadings, which is much thicker than the state of the art electrodeposited values (around a few microns). Secondly, depending on the catalytic processes, highly reducible noble metals such as Rh^{3+} are incorporated into the HT structure. Such incorporation makes the electrodeposition process more complicated. Lastly, the simultaneous electrodeposition of multiple components generates a challenge in the control of the composition.

This paper provides an overview of the electrodeposition of HT materials onto FeCrAlloy open-cell foams. After calcination at high temperature, the samples were used as structured catalysts for syngas ($CO + H_2$) production from CH_4 via steam reforming (SR) or catalytic partial oxidation (CPO) processes. It is focused on two aspects: (i) the fundamental understanding of the electrochemical-chemical reactions that are most relevant for the electrodepositions of HT compounds (OH^- generation and consumption), using the simple case of Mg/Al HT phases as an example, and (ii) the demonstration of the influence of synthesis parameters on the properties of the structured catalysts obtained by electrodeposition of Ni/Al and Rh/Mg/Al HT compounds and, hence, on their catalytic performance for the SR or the CPO of CH_4 .

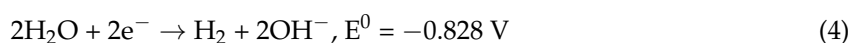
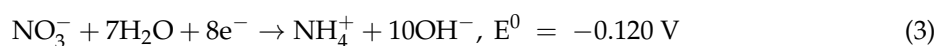
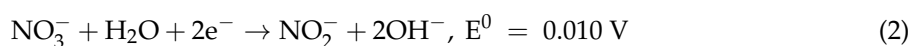
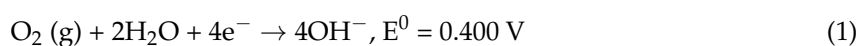
2. Reactions Involved in the Electrodeposition of HT Compounds and Nitrate Concentration Effect

The electro-base generation method for the deposition of HT compounds is based on the application of a cathodic pulse at the foam dipped in a solution containing nitrates and divalent and trivalent cations. In the preparation of Mg/Al HT compounds, $Mg(NO_3)_2$ and $Al(NO_3)_3$ aqueous solutions with different Mg^{2+}/Al^{3+} ratios and total metal concentrations can be used, also containing KNO_3 as supporting electrolyte. The production of OH^- ions by electrochemical reactions and their consumption by chemical precipitation occur simultaneously at the vicinity of the structured support. It is necessary to reach the target pH values to obtain HT compounds with well-controlled composition

and to avoid side-phase precipitations [52]. Since both electrochemical and chemical processes proceed concurrently in a short time and are inter-related, a work was performed to better understand these processes and a possible modification during the electrodeposition pulse.

Potential sweeps or pulses were applied at FeCrAlloy foams (80 ppi) dipped in electrolytes of different composition [53]. The cathodic nitrate reduction was investigated in the absence and presence of precipitating cations, i.e., 0.135 M KNO_3 , or $\text{Mg}(\text{NO}_3)_2$ and $\text{Al}(\text{NO}_3)_3$ with $\text{Mg}/\text{Al} = 3/1$ as atomic ratio (a.r.) and 0.06 M total metal concentration, respectively. The concentration of the nitrates was kept constant in both solutions. The contribution of water reduction was analyzed using nitrate-free electrolytes; i.e., solutions containing chlorides (KCl or MgCl_2 and AlCl_3) at the same total concentration as the nitrate solutions. The role of O_2 reduction was evaluated using de-aerated solutions. All the experiments were performed in a single compartment cell, where the foam was the working electrode, the counter electrode was a Pt mesh and the reference electrode a saturated calomel electrode (SCE). Moreover, pH measurements were carried out by a micro pH electrode inserted inside the foam cylinders.

The results confirmed that nitrate, water and O_2 reduction contribute to the pH increase at the foam electrode-electrolyte interface according to the following reactions:



OH^- generation from dissolved O_2 has a minor contribution, due to its low concentration in the solution, while H_2O and NO_3^- reduction were competitive to become a dominant contributor. Although both reactions contributed to increase the pH, the former formed H_2 bubbles giving a negative effect on the adhesion of the coating and the pH generated was low. For instance, the pH reached near the foam after the application of a -1.2 V vs. SCE potential for 2000 s was around 2 units lower when nitrates were absent in the bath. A solution containing chloride precursors reached a pH around 6.5, while in the presence of nitrates the pH went up to 8.5 at the plateau (Figure 1a). Consequently, in a chloride bath a thin coating with Mg/Al ratio only around 0.6/1 was deposited, a value much lower than the 3/1 nominal one. Conversely, in the nitrate bath a thicker deposit of materials containing both Mg^{2+} and Al^{3+} at a higher ratio was obtained as characterized by scanning electronic microscopy (SEM) coupled with energy-dispersive X-ray spectroscopy (EDS) (Figure 1b, c). These results confirmed the key role of nitrates in the generation of a pH suitable for the precipitation of HT compounds with a controlled composition.

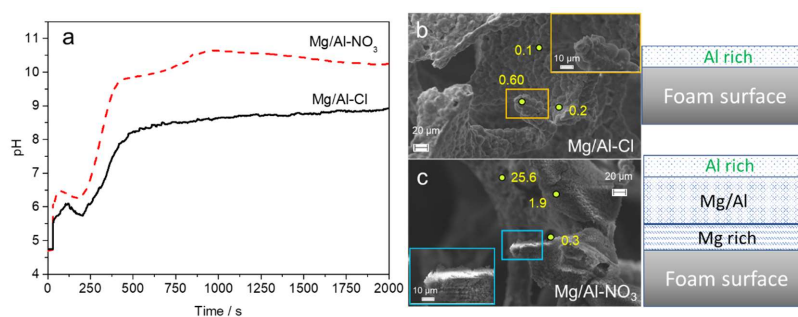


Figure 1. (a) Evolution of the pH near the foam surface dipped in 0.06 M $\text{Mg}/\text{Al-Cl}$ and 0.06 M $\text{Mg}/\text{Al-NO}_3$ solutions during the current transient curve (-1.2 V vs. SCE for 2000 s); (b,c) SEM images of the respective coatings. The numbers in SEM images are the Mg/Al ratio values recorded for some regions of interest. Adapted from [53].

It should be remarked that linear sweep voltammetries (LSVs) performed in the alloy dipped in a solution without precipitating cations, i.e., in only KNO_3 , displayed a low activity in nitrate reduction (Figure 2). The analysis of the solution withdrawn near the foam surface revealed that both NO_2^- and NH_4^+ were produced. The Mg^{2+} and Al^{3+} precipitating cations, and especially Al^{3+} , shifted the onset potentials to less cathodic values and increased the current density (Figure 2). The 2 or $8e^-$ reduction processes, and, therefore, the amounts of NO_2^- and NH_4^+ produced, depended on the applied potential, time, and presence of cations. Remarkably, it was found that along the 2000 s pulse in the presence of Mg^{2+} and Al^{3+} , NO_2^- production decreased. This behavior was probably due to the presence of Al^{3+} , since NO_2^- production rose in the case of sole $\text{Mg}(\text{NO}_3)_2$ electrolyte. It should be noted that the nitrate reduction products depend on the pH [54]. For example, a low pH is more conducive to ammonia reduction while a high pH favors the reduction to NO_2^- . Therefore, the dependence of $\text{NH}_4^+/\text{NO}_2^-$ ratio on electrochemical parameters, such as potential and time, may give some lights to explain as well as to control better the characteristics of the coating (loading, composition), which are associated with the pH values near the cathode surface.

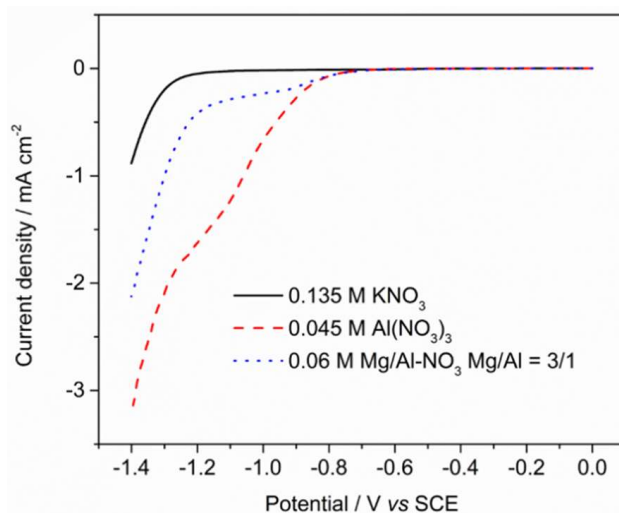


Figure 2. LSV curves recorded at the FeCrAlloy plate dipped in 0.135 M KNO_3 , 0.045 M $\text{Al}(\text{NO}_3)_3$, and 0.06 M $\text{Mg}/\text{Al}-\text{NO}_3$ solutions. Scan rate: $1 \text{ mV}\cdot\text{s}^{-1}$; Potential range: 0 to -1.4 V . Adapted from [53].

Since nitrate reduction plays a key role in OH^- generation, the effect of nitrate concentration on both electrochemical and chemical processes were investigated [55]. Mg/Al HT compounds were deposited using Mg/Al nitrate baths ($\text{Mg}/\text{Al} = 3/1$ a.r.) of different total metal concentration (0.03, 0.06 and 0.10 M) and potential pulses of different lengths (100, 1000, and 2000 s). For comparison purposes, experiments were performed in KNO_3 solutions containing nitrate concentrations equal to those deriving from the metal salts (0.0675, 0.135, and 0.225 M). The reduction processes followed a surface reduction behavior at short times (below 500 s) in the nitrate concentration range from 0.0675 to 0.225 M (Figure 3a). They were slowed down by the solid deposition or the ineffective solution replenishment at the electrode interface, being more remarkable with more concentrated baths (Figure 3b).

The metal nitrate concentration determined both OH^- generation by nitrate reduction and OH^- consumption by precipitation of cations. The SEM/EDS analysis and the characterization of crystalline phases and intercalated anions on the coatings by X-ray diffraction (XRD), attenuated total reflection (ATR) and micro-Raman revealed that the metal nitrate concentration governed: (i) the quality of the coating (e.g., the amount of solid deposited and its distribution on the foam); and (ii) the properties of electrodeposited materials (e.g., the solid growth mechanism, crystallinity of the phases and intercalating anions inside the HT structure) (Figure 4). A low concentration produced thin coatings unevenly distributed over the foam surface, while a high concentration led to the pore

blockage. The main drawback of the method was the uncontrolled precipitation as the synthesis time increased. Consequently, at 2000 s the coatings were made by stratified layers of different composition and morphology (see scheme in Figure 4). HT-, brucite-type phases and Al-rich layers (probably also gibbsite) were identified. The concentration of the bath modified: (i) the crystallinity of the phases, (ii) the arrangement of nitrate anions inside the HT phase, (iii) the size of $\text{Mg}(\text{OH})_2$ or Mg-rich platelet particles, and (iv) the growth of the Al-rich layer. The increase in the concentration from 0.03 to 0.10 M favored the formation of larger and more crystalline $\text{Mg}(\text{OH})_2$ particles near the foam surface, poorly crystallized HT phases nitrate intercalated with a higher interlayer region, and fostered the formation of the Al-rich outer layer. The Al-rich layer probably deposited due to the ineffective replenishment of the solution near the foam surface and the formation of an insulating layer during the electrodeposition.

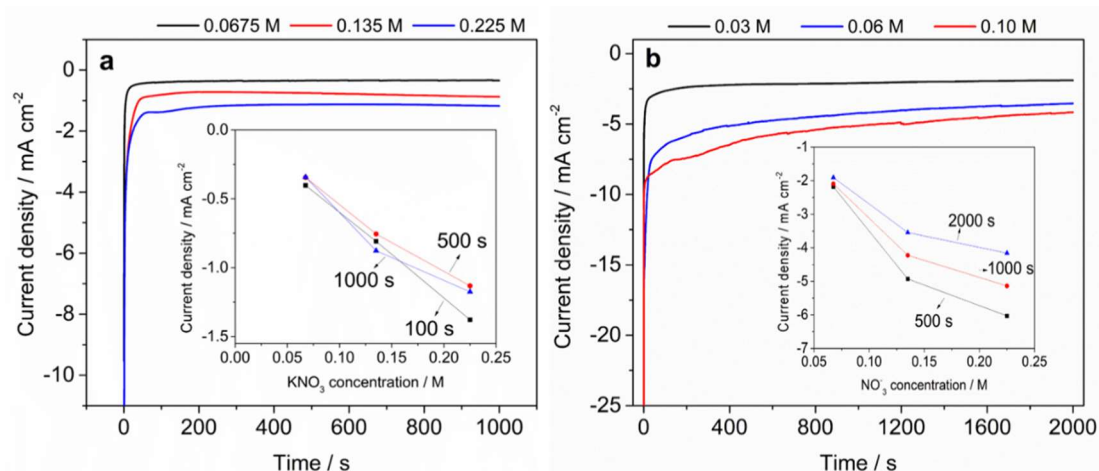


Figure 3. Current transients recorded at FeCrAlloy foams at -1.2 V vs. SCE in (a) KNO_3 and (b) $\text{Mg}/\text{Al}-\text{NO}_3$ ($\text{Mg}/\text{Al} = 3/1$) solutions. The insets present the dependence of current densities on total nitrate concentration at different times. Adapted from [55].

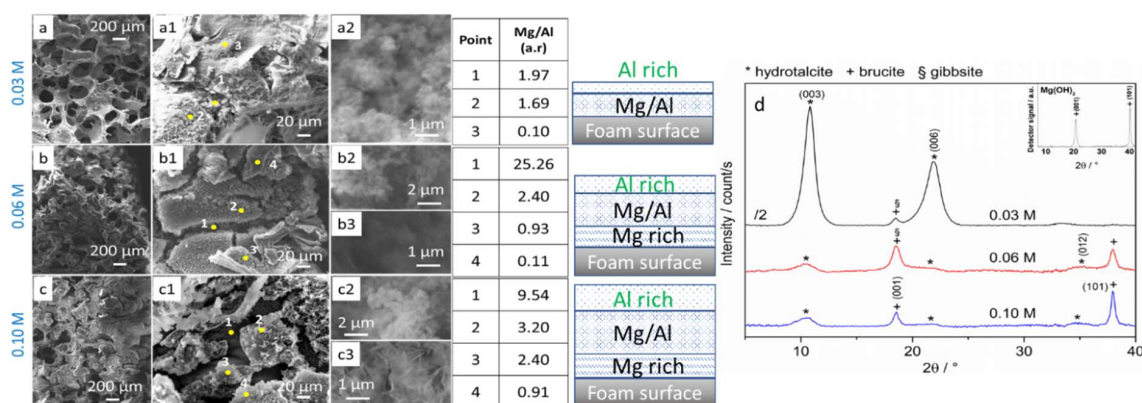


Figure 4. Effect of total metal nitrate concentration on the properties of the Mg/Al HT coatings on FeCrAlloy at -1.2 V vs. SCE for 2000 s. SEM images of coated foams: 0.03 M (a,a1,a2), 0.06 M (b,b1–b3), and 0.10 M (c,c1–c3), and (d) XRD patterns of coated plates. The table summarizes Mg/Al ratios obtained from EDS spectra in the regions of interest indicated by the numbers. Adapted from [55].

The metal nitrate reduction played a key role in the electrodeposition, a balance being achieved between the generation of the OH^- by electrochemical reduction processes and the OH^- consumption by precipitation reactions to control not only the amount of solid but also the composition and structure. These coating properties are of paramount importance during the preparation of structured catalysts. They will determine the amount of catalyst and the dispersion of the active phase in the

brucite structure of the as-deposited materials and consequently the same properties in the calcined structured catalysts.

3. Effect of Electrosynthesis Parameters in the Preparation of Ni/Al and Rh/Mg/Al HT Materials for Structured Catalysts

For catalytic applications in the production of H₂ and syngas by SR and CPO of CH₄, Mg²⁺ is replaced by Ni²⁺ and/or Rh³⁺ in the brucite-type layers [56]. The actual structured catalyst is obtained by calcination at high temperature (900 °C). A highly active and well-adhered layer as well as a stable metallic foam are mandatory to achieve high catalytic performances. In the deep study performed for the preparation of structured catalysts by electrodeposition of HT compounds we realized that the coating of complex metallic foam structures with such HT catalyst precursors faced several issues to reach a target catalytic film that included not only the metal nitrate concentration. The quality of the coating was determined by: (i) the support, including nature (electrical conductivity and roughness [57]) and geometrical parameters (size and shape [58]); (ii) electrochemical set-up (electrical contact between the working electrode and the potentiostat [59] and type of cell [60]); (iii) electrochemical parameters (precursors, concentration and pH of the electrolyte, applied potential, and synthesis time [58,61–63]); (iv) the interaction of coating with the metallic support [64]. The nature of the support and geometrical parameters are usually fixed by foam suppliers or given catalytic purposes, while the electrochemical set-up and parameters can be varied to control the coating properties. In the following sections we will summarize how the parameters were modified to prepare HT-precursors of Ni/Al, Rh/Mg/Al and Rh/Ni/Mg/Al catalyst, paying special attention to the characterization of the structured catalysts at the three stages of their life-time (after electrodeposition, calcination and catalytic tests).

3.1. Ni/Al Catalysts

Ni/Al HT precursors were electrodeposited on FeCrAlloy foams (1.2 cm diameter, 80 ppi) starting from a solution containing Ni(NO₃)₂ and Al(NO₃)₃ (Ni/Al = 3/1 a.r.), 0.03 M total metal concentration, with KNO₃ as supporting electrolyte. The samples after calcination at 900 °C and reduction in a H₂/N₂ mixture at 750 °C were proposed as structured catalysts for SR of CH₄ [48,57,62]. The electrodeposited solid loading, homogeneity and composition depended on the applied potential (−0.9 and −1.2 V vs. SCE) and synthesis time (600, 1000, and 1800 s). The former controlled the pH close to the foam surface, while the latter determined the coverage degree of the foam and the film thickness. Consequently, both electrochemical parameters controlled the composition of the film and, therefore, the amount and distribution of the Ni active sites.

A −0.9 V vs. SCE potential did not provide a pH high enough for the precipitation of the HT material, despite successful results were previously obtained in the deposition of Ni/Al compounds on Pt electrodes [65]. Hence, the generation of a pH close to the foam was lower than the one obtained at the Pt support. Consequently, a film containing the most acidic cation, i.e., an Al-rich solid, precipitated. Moreover, the film coverage and Ni-content increased with the synthesis time from 600 to 1800 s. It should be remarked that the deposition first took place on the most exposed areas. In contrast, the more cathodic −1.2 V vs. SCE potential generated a suitable pH for the formation of the Ni/Al HT, therefore improving the coating properties. The sample prepared after 1000 s showed a higher coating quality in terms of solid amount and stability (Figure 5a). Namely, a quite good control of the composition of the deposited thin film (1–2 μm) was achieved, Ni/Al was around 2.8/1 (identified by inductively coupled plasma atomic emission spectroscopy (ICP-AES) analysis) compared to the 3/1 nominal one.

The chemical-physical characterization of the thin deposits on the complex foam support was challenging. The preliminary characterization by XRD and FT-IR (fourier-transform infrared spectroscopy) of electrodeposits over FeCrAlloy plates confirmed the formation of the HT phase intercalated with nitrate anions. After calcination at 900 °C, the more powerful μ-XRD/XRF (micro

X-ray diffraction/X-ray fluorescence) synchrotron tomography allowed to characterize the as-prepared coatings [66]. The characterization of the spatial distribution of the elements and crystalline phases revealed that they were made of NiAl_2O_4 and NiO phases, characteristic of HT-derived catalysts (Figure 5b), and in agreement with H_2 -TPR (hydrogen temperature programmed reduction) results. The resolution of the technique allowed to state that the electrodeposition was also taking place in the cavities of the foam. Moreover, an alumina scale developed between the foam and the catalytic coating, due to the foam oxidation, and K-containing phases were also identified. The crystalline structure of the catalyst was modified during the reduction pretreatment and catalytic tests; and the active catalyst was instead formed by Ni^0 dispersed on $\gamma/\eta\text{-Al}_2\text{O}_3$ that homogeneously coated the FeCrAlloy foam surface. Despite the formation of a thin coating, the structured catalyst exhibited catalytic performances comparable with those of a Ni-containing commercial catalyst under industrial-type conditions, i.e., $S/C = 1.7$, $P = 20$ bar, $\tau = 4$ s, and $T_{\text{oven}} = 900$ °C (Figure 5c). These results confirmed the advantages of using structured catalysts based on metallic foams such as enhanced heat transfer and increased effectiveness factor, leading to a better utilization of the catalyst.

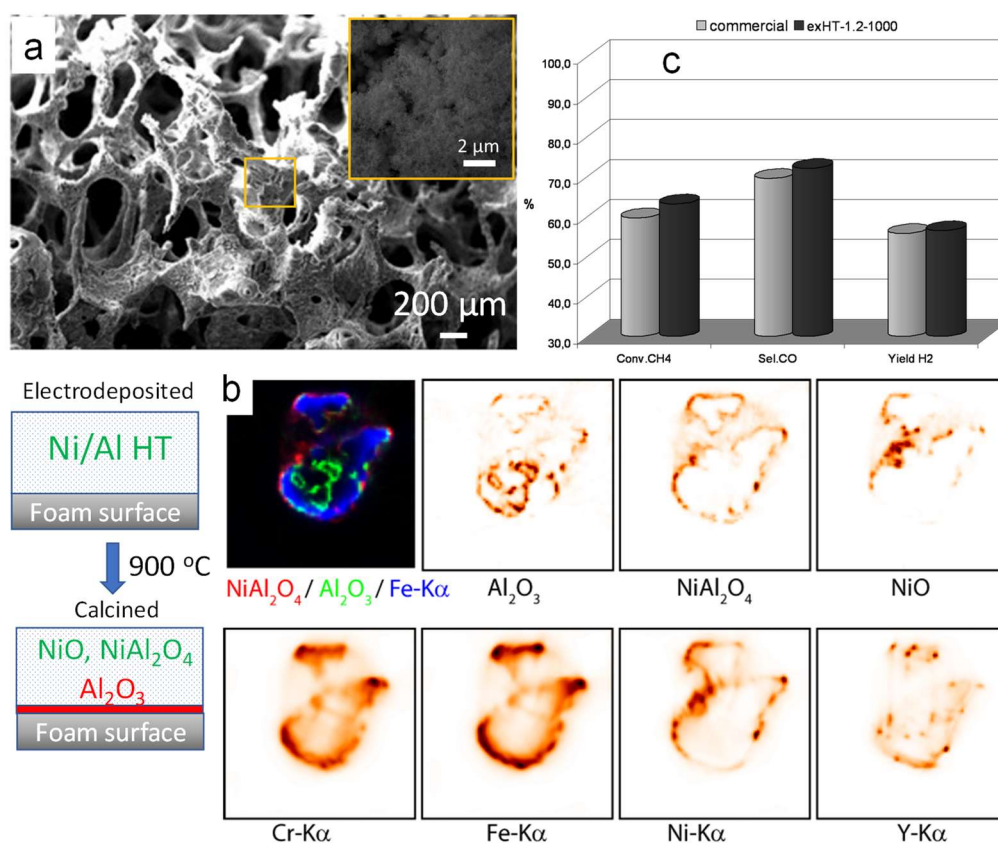


Figure 5. Properties and catalytic activity of Ni/Al HT-derived catalysts coated on FeCrAlloy foam at -1.2 V vs. SCE for 1000 s and calcined at 900 °C for 12 h. (a) SEM images, (b) μ -XRF/XRD tomography images: elemental (lower row) and phase (upper row) maps obtained by XRF/XRPD tomography [240 μm (3 μm steps) \times 180° (2° steps)]. Identification by comparison with the ICDD PDF-2 database yields: Al_2O_3 (75–1862), NiAl_2O_4 (73–0239) and NiO (89–7390), (c) Catalytic activity for SR of CH_4 at $P = 20$ bar, $S/C = 1.7$, $T_{\text{oven}} = 900$ °C, contact time $\tau = 4$ s. Figure 5a was adapted from [62], Figure 5b from [66] and Figure 5c from [48].

3.2. Rh/Mg/Al Catalysts

3.2.1. pH of the Electrolyte, KNO₃ Supporting Electrolyte and Synthesis Conditions

Rh-containing HT compounds are very active in H₂ production processes such as the CPO of CH₄. However, the electrodeposition of this type of HT materials is rather challenging. Noble metals are easily reducible and the deposition of Rh metallic particles using similar electrodeposition conditions as for Ni/Al HT compounds took place, i.e. electrodepositions in an 80 ppi foam (8.0 × 10.0 mm cylinder) at −1.2 V vs. SCE for 1000 s with a 0.03 M Rh/Mg/Al = 11/70/19 a.r.% electrolyte containing 0.3 M KNO₃ supporting electrolyte, pH 2.1 [61]. This led to the deposition of a film with uncontrollable composition and to the formation of big Rh⁰ particles (Figure 6a), which were less catalytically active due to poor dispersion. To avoid this drawback, the initial pH of the electrolyte was increased. The increase of the pH lowered the reduction Rh³⁺ potential according to the Pourbaix diagram; however, it should be noted that it may also lead to the precipitation of the acidic Al³⁺ cations as bulk aluminum hydroxides (Al(OH)₃) or oxohydroxides (AlOOH). An initial pH value of 3.8 of the electrolyte balanced both issues. Under these conditions, the presence of Rh³⁺ did not modify the electrodeposition process at −1.2 V vs. SCE for 2000 s (Figure 6b). The current density recorded during the synthesis, in the absence or presence of Rh in Mg/Al electrolyte solution, and properties of the coatings were quite similar [60]. Moreover, Rh⁰ species were not identified by powerful μ-XANES (X-ray absorption near edge structure) measurements of the as-deposited coating [63].

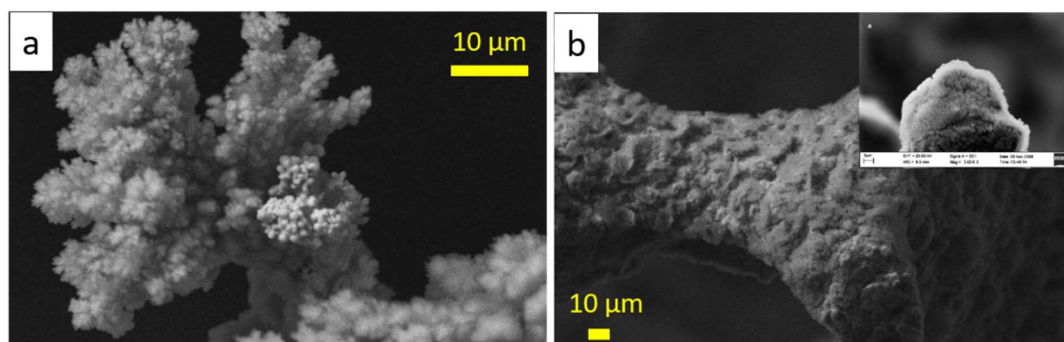


Figure 6. SEM images of Rh/Mg/Al coating on FeCrAlloy foam electrodeposited at −1.2 V vs. SCE in 0.03 M Rh/Mg/Al = 11/70/19 a.r.% and 0.3 M KNO₃ at different synthesis conditions: (a) 1000 s and pH 2.1 (without adjusting the pH), (b) 1000 s and pH 3.8. The pH was adjusted by NaOH. Adapted from [61].

Once adjusted the pH of the initial solution, applied potential and syntheses time were optimized to deposit Rh/Mg/Al = 11/70/19 a.r.% HT precursor, starting from a 0.03 M total metal concentration and 0.3 M KNO₃ [58]. The challenges of the method were evidenced again since the syntheses conditions were related to the foam cylinder size. Increasing the size of the cylinder from 8.0 × 10.0 to 10.0 × 11.9 mm, a longer synthesis time was required to improve the coating homogeneity and layer thickness. Under these long synthesis times, a −1.3 V vs. SCE potential was not suitable, because of the evolution of H₂ bubbles with the detachment of the deposited solid. On the other hand, it was possible to work at −1.1 V and −1.2 V vs. SCE. The application of a lower cathodic potential, however, decreased the pH value and slowed down the OH[−] generation, decreasing the precipitation rate. To balance this effect, the synthesis time was adjusted: 3000 s at −1.1 V and 2000 s at −1.2 V. A 3 wt.% solid deposited in both cases. However, some inhomogeneities in the deposition process were observed regardless of the potential applied: the electrodeposition was favored on the tips of the struts rather than on the nodes because the generation of potential gradients and the more favored heterogeneous precipitation in the most exposed areas.

The calcination at 900 °C for 12 h to obtain the catalyst was another process that altered the properties of the coating. The weight losses due to the removal of water, CO₂, and NO_x during

dehydration, dehydroxylation and interlayer anions decomposition led to the shrinkage of the coating. Moreover, metal and oxides have different thermal expansion coefficients. Thus, the calcination process contributed to crack formation. The catalysts after reduction at 750 °C for 2 h in a H₂/N₂ mixture were tested in the CPO of CH₄, feeding CH₄/O₂/He gas mixtures to the reactor loaded with two coated foams. The oven temperature was 750 °C, the composition of the gas mixture (CH₄/O₂/He = 2/1/20 and 2/1/4 v/v) and the gas hourly space velocity (GHSV) value (63,300–11,500 h⁻¹) were modified. The performances were higher with the catalyst prepared at -1.2 V, although it still showed low performances (e.g., CH₄ conversion around 70%) in comparison with pelletized catalysts due to some uncoated zones, a low Rh dispersion, and the presence of potassium in the spent catalyst.

The electrodepositions were performed in the presence of KNO₃ as supporting electrolyte to increase the conductivity of the solution (and, hence, to reduce Ohmic drop resistance) or to eliminate the contribution of migration of the electroactive species [67]. Unfortunately, K⁺ had a high tendency to migrate toward the working electrode and, thus, to simultaneously deposits with the HT compounds (Ni/Al and Rh/Mg/Al). Potassium is reported to be a catalyst promoter decreasing the carbon formation; however, in this case the deposition of large amounts led to the blockage of the active sites and decrease of the performances. Thus, electrodepositions were performed without KNO₃; however, the absence of the supporting electrolyte could modify the electro-based generation. In KNO₃-free electrolytes a reduced number of nitrates was available to increase the pH and, therefore, the coating morphology and composition, which determined the catalytic properties, were modified as shown below.

The electrodeposition without KNO₃ at -1.1 V favored the precipitation of the most acidic cations (Rh³⁺ and Al³⁺) due to lower pH, with lower amounts of Mg-containing coatings. Consequently, after calcination the catalyst was made of rhodium oxide on alumina in the areas poorer in magnesium and/or within a magnesium oxide or magnesium spinel matrix when the magnesium content increased. The different phases in the catalyst modified not only the inherent properties of the coating (i.e., Rh dispersion, stability against sintering, carbon formation), but also its adherence, of paramount importance to keep stable performances. By applying a more cathodic potential, i.e., -1.2 V, the coverage of the foam was more homogeneous, but another drawback was identified: a sequential precipitation took place, i.e., a Mg-rich layer deposited close to the foam surface and a large amount of Al and Rh did it in the outer shell of the coating. Consequently, after calcination the catalyst still contained several Rh species; however, the contribution of those with Mg was more intense than in the sample obtained at -1.1 V. The catalyst did not show optimal performances yet, but they were improved. The more homogeneous foam coating, together with the enrichment in Rh-containing species, due to the sequential precipitation, may be responsible for these improved performances. Conversion increased from 75 to 85% (GHSV 63,300 h⁻¹), although the catalyst deactivated by feeding concentrated gas mixtures (CH₄/O₂/He = 2/1/4 v/v) at 750 °C. The sintering and oxidation of Rh⁰ active species could contribute to the still low activities and the deactivation, thus the method was further improved to overcome these drawbacks.

As above commented, the properties of the structured catalysts were not only related to the deposited solid but also to the calcination process. Besides weight losses and thermal expansion coefficients, the evolution of the coating and the foam during calcination played an important role on the properties of electrodeposited structured catalysts [64]. The calcination modified not only the coating properties but also the metallic foam, i.e., the foam was oxidized developing an alumina scale. Thus, during the calcination, the interaction between the metallic support and the catalytic coating occurred: a chemical reaction between Al from the foam and Mg in the coating. This interaction had a twofold effect, it increased the film adhesion during the thermal treatment and catalytic tests but modified the catalyst crystalline phases. Spinel phases in which rhodium was solved developed, thus decreasing the catalyst reducibility, they coexisted together with some Rh₂O₃ and Rh⁰. The metallic support was oxidized forming the corundum scale, which did not completely cover the foam surface, and chromium oxides, together with ι -Al₂O₃.

The coatings obtained under the above reported electrodeposition conditions showed some inhomogeneities: (i) the tips of the struts were usually coated by thicker films than zones connecting the struts; (ii) the outer part of the foam cylinders was better coated than the inner one; and (iii) a sequential precipitation was observed for all long syntheses times. The inhomogeneous coating of the foam cylinder may be related to the electrical-resistance of the metallic material. Hence, the electrical contact was modified to achieve homogeneous thicknesses; the number of electrical contacts (pin) obtained by inserting a Pt wire in the foam was increased [59]. The increase in the efficiency and uniformity of the current distribution moving from one to three electrical contact point configuration led to improvements. A more homogeneous coating of FeCrAlloy foams was obtained at -1.1 V for 3000 s and -1.2 V for 2000 s. Furthermore, enhanced coating properties were also observed after calcination. However, the sequential precipitation was not avoided. The outer layer rich in Rh and Al layer was less stable during reaction conditions and it could be partially detached. The lower stability of the outer layer both during calcination and catalytic tests in the sample prepared at -1.2 V led to a decrease in catalytic performances, while in the sample prepared at -1.1 V for 3000 s the increase in the homogeneity of the film led to better performances with the 3-pin configuration.

3.2.2. Rh Loading, Electrolyte Concentration and Bimetallic Catalysts

The initial development of the electrodeposition of Rh-containing HT compounds on FeCrAlloy foams above reported was performed by depositing a highly Rh loaded HT phase (Rh/Mg/Al = 11/70/19 a.r.%) to balance the amount of active sites due to the small amount of coating; the coating thickness was low (5–15 μm on the tips of the struts and several plate zones, 2–6 μm on other parts, as well as a few scarcely coated surfaces). Moreover, the coating film was not homogeneous, being composed by an inner and outer layer, differing in composition. Hence, a further step for the optimization of the technique was to reduce the amount of Rh in the film, without decreasing performances, by tailoring the Rh particle size, coating thickness and active phase composition.

To reduce the metal particle size and the sintering, the Rh/Mg/Al a.r.% in the electrolytic solution was decreased from 11/70/19 to 5/70/25 and 2/70/28 (Figure 7) [63]. A change of Rh amount in the electrolytic solution did not alter the typical features of electrodeposited precursors and catalysts, but did determine the Rh dispersion. The precipitation of a solid with a composition close to the expected one at the beginning of the syntheses, followed by the deposition of a film enriched in Al and Rh (outer layer) still occurred. However, the Rh loading was proportional to the Rh content in the electrolyte. After calcination, the outer layers in thick coated zones (5–15 μm) developed a high number of cracks and the solid easily detached as previously observed, whereas Mg-rich coatings or those with well-defined composition were more stable. The Rh speciation did not largely change with the Rh content. The characterization of the coatings by $\mu\text{-XRF/XANES}$ indicated the presence of hardly reducible $\text{Mg}(\text{Rh}_{1-x}\text{Al}_x)_2\text{O}_4$. Nevertheless, after reduction and catalytic tests, the particle size and dispersion depended on the Rh loading and coating thickness. Smaller and more dispersed particles were obtained by decreasing the Rh concentration in the electrolytic solution; these particles were found in thinner rather than thicker layers, since in the former the Rh amount deposited was lowered (Figure 7a–c). However, the catalytic activity in the CPO of CH_4 at 750 °C with diluted and concentrated feedstocks ($\text{CH}_4/\text{O}_2/\text{He} = 2/1/20$ and $2/1/4$ v/v) was shown to be mainly related to the Rh content rather than to the metallic particle size (Figure 7e). Despite the decrease in metallic particle size, the CH_4 conversion was negatively affected by the low number of active sites in the coating, the high metal support interaction and, probably, the oxidation of metallic particles and carbon formation.

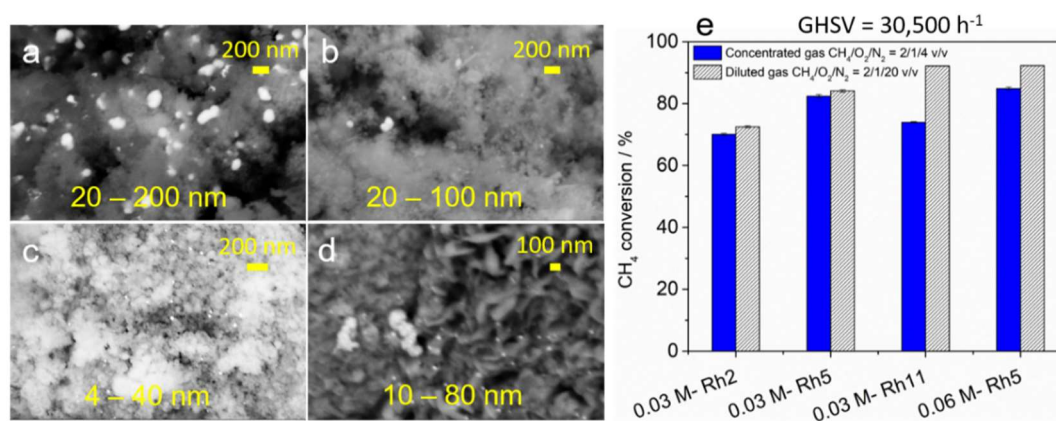


Figure 7. Field emission gun scanning electron microscopy (FEG-SEM) images of Rh spent catalysts: (a) 0.03 M, Rh/Mg/Al = 11/70/19 (a.r.), (b) 0.03 M, Rh/Mg/Al = 5/70/25, (c) 0.03 M, Rh/Mg/Al = 2/70/28, (d) 0.06 M, Rh/Mg/Al = 5/70/25, and (e) CH₄ conversion of the catalysts in the catalytic partial oxidation at $T_{\text{oven}} = 750\text{ }^{\circ}\text{C}$, $35,000\text{ h}^{-1}$ and feeding diluted and concentrated feedstocks. The syntheses were performed at -1.2 V vs. SCE for 2000 s and pH 3.8. The catalysts were calcined at $900\text{ }^{\circ}\text{C}$ for 12 h. Adapted from [63].

To further increase the activity of the catalysts prepared from an electrolyte with a lower Rh loading (Rh/Mg/Al = 5/70/25 a.r.%), the total metal concentration was increased from 0.03 M to 0.06 M. This electrolytic solution allowed to precipitate a thicker layer, 15–20 μm on struts and around 5 μm on flat zones (nodes). The composition was close to the expected one (Rh/Mg/Al = 4/68/28 a.r.%) in some parts of the foam, but the sequential precipitation phenomena still took place where thicker layers were obtained, following a behavior similar to that observed for Mg/Al compounds. Despite the electrodeposited sample still showed some uncontrolled properties, in the calcined and reduced catalyst, the presence of a thicker layer with a high number of active sites, but without altering the growth and sintering behavior of Rh⁰ particles (Figure 7d), gave rise to an increase in the performances. Compared to the catalyst prepared from 0.03 M (as total concentration) to the one from 0.06 M solution showed a higher CH₄ conversion in all reaction conditions, about 10% and 4% higher in diluted and concentrated feeds, respectively (Figure 7e).

Another alternative to enhance the catalytic activity without increasing the Rh loading was the deposition of a HT compound where Mg²⁺ cations were partially replaced by Ni²⁺ (Rh/Ni/Mg/Al = 5/15/55/25 a.r.%). Ni-catalysts are also active in the CPO, and Ni activity is increased in the presence of Rh. However, the electrodeposition of such a type of HT material was highly challenging. Although a better coverage degree was achieved, several layers of solid were identified in SEM images, whose composition seemed to be related with the precipitation pH of the individual hydroxides. Despite these features, a very active bimetallic Rh/Ni catalyst was obtained; CH₄ conversion and selectivity to syngas were above 90% at all the operative conditions ($\text{GHSV} = 11,500\text{--}63,300\text{ h}^{-1}$, for both diluted and concentrated feeds), although it slightly deactivated with time-on-stream.

Step by step the electrodeposition was optimized; however, the two main drawbacks that still limited its applicability were: (i) the lack of control in the composition of the deposited solid, which determined both the metallic particle size and the adhesion of the film during calcination and catalytic tests, and (ii) inhomogeneity in the coverage of both inner and outer surfaces of the foam cylinder. An interplay among the local pH values reached in the closeness of the support surface, the increase in the resistivity of the system as the surface was coated by hydroxides, and the diffusion of the electroactive species (nitrates) and cations to the working electrode must be considered to explain the sequential precipitation. While inhomogeneity in the coverage of inner and outer surfaces could be

explained by the limited mass transfer inside the pores. All these issues may be related to the static electrolytes during the electrodeposition.

3.2.3. Double compartment Flow Cell

All the aforementioned studies were performed by coating the foams in a single compartment electrochemical cell operating under static conditions. Although this cell is widely used for electrochemical experiments, it may have two main drawbacks for the electrodeposition on complex-shaped and quite large size electrodes, such as open-cell foams. The first one is that this configuration does not avoid the mixing between the products from the counter and the working electrodes. The second disadvantage is the inefficient replenishment of the electrolyte in the electrode/electrolyte interface. To tackle these issues, in our recent work [60], a double-compartment flow cell was used for the electrodeposition of Rh/Mg/Al HT on FeCrAlloy foams. The experiments were carried out under the same electrochemical conditions, i.e., 0.06 M nitrate solutions containing the lowest Rh loadings, i.e., Rh/Mg/Al = 5/70/25 and 2/70/28 a.r.% at -1.2 V vs. SCE for 2000 s with an electrolyte flow of $2 \text{ mL}\cdot\text{min}^{-1}$.

Successfully and regardless of the Rh content, Rh/Mg/Al HT precursors (4.6 wt.% loading) with controlled composition and thickness around $5\text{--}20 \mu\text{m}$ were evenly deposited on the surface of FeCrAlloy struts (Figure 8a,b). Only some deviations were found in a few regions where Mg-rich and Al-rich layers precipitated. Moreover, very thin layers (less than $1.5 \mu\text{m}$) coated the cavities within the struts, thus increasing the catalytic surface area.

The control in the composition of the electrodeposits had a direct effect on the calcined and reduced catalysts. The morphology and size of the catalyst particles after calcination were not largely altered and the film showed a smaller number of cracks and detachments than in the previous works. The absence of Rh- and Al-rich layers, which easily detached, and the interaction between the support and coating as well as the stability of HT compounds during calcination could explain this improvement (Figure 8c,d). Thus, the catalysts prepared were similar to those obtained by the conventional coprecipitation method. To confirm this statement, the crystalline phases in the coating were investigated by nano-XRF/XRD. Likewise, for the characterization of Ni/Al coatings the spatial distribution of the elements and crystalline phases were obtained; however, in this study the spatial resolution of the results was increased. The measurements confirmed that the coatings were mainly made of MgO and MgAl_2O_4 phases with Rh^{3+} species well dispersed, characteristic of coprecipitated HT-derived catalysts. Moreover, a MgAl_2O_4 film developed at the interface between the foam and the coating due to the chemical interaction between Mg^{2+} from the coating and Al^{3+} from the support, which increased the adherence to the support (Figure 8e).

The coating after reduction and catalytic tests also showed enhanced properties: (i) good stability characterized by SEM and nano-XRF/XRD; (ii) low tendency to form carbon evidenced by micro-Raman; and (iii) well-dispersed Rh^0 particles with an average size of $2\text{--}3 \text{ nm}$ as observed by high-resolution transmission electron microscopy (HRTEM) (Figure 8g), which coexisted with some Rh aggregates of $15\text{--}30 \text{ nm}$. These properties provided active and stable performances for the Rh/Mg/Al = 5/70/25 (a.r.%) catalyst. The activity was close to those obtained with coprecipitated catalysts in the CPO of CH_4 under different reaction conditions (i.e., feeding diluted and concentrated feedstock and at 750 and $500 \text{ }^\circ\text{C}$, as well as during long tests) (Figure 8f). However, a thicker coating should be necessary to achieve similar performances with the Rh/Mg/Al = 2/70/28 (a.r.%) catalyst to balance the number of active species.

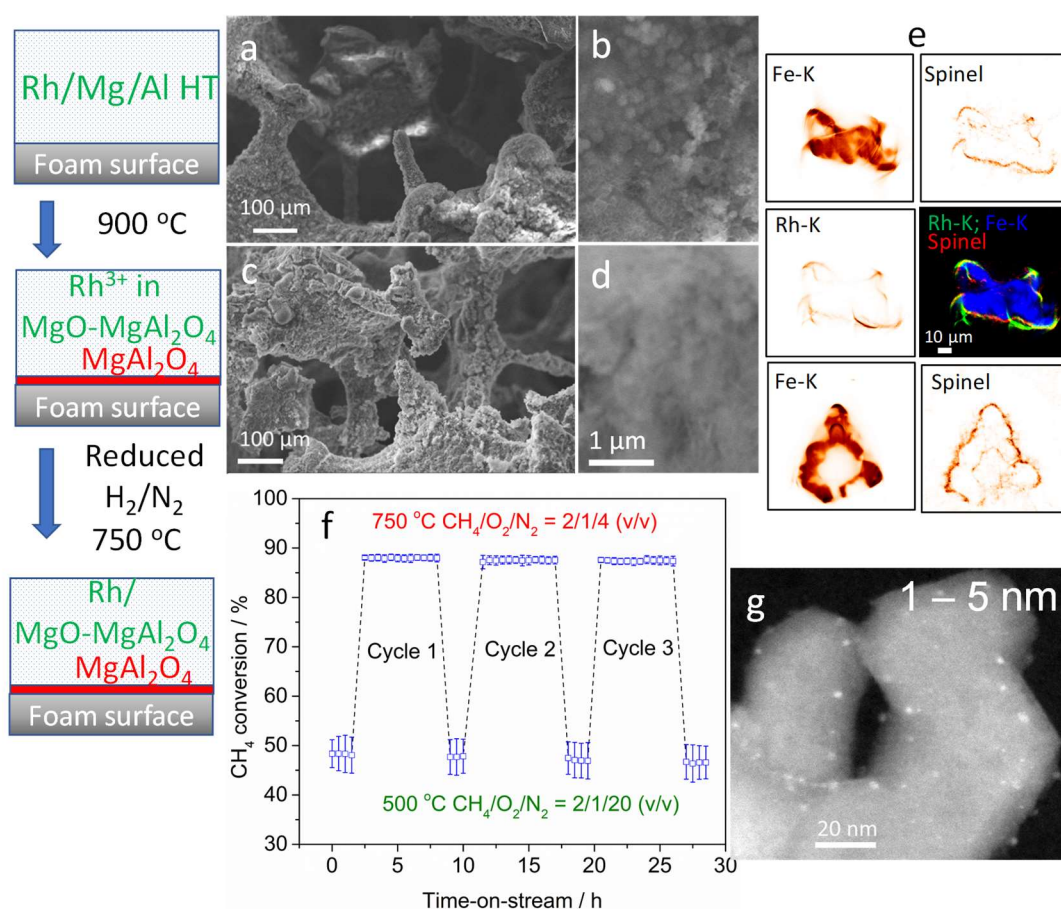


Figure 8. Properties Rh/Mg/Al structured catalysts electrodeposited from 0.06 M electrolyte in a double-compartment flow cell, Rh/Mg/Al = 5/70/25 (a.r.%) nitrate solution (pH 3.8) at -1.2 V vs. SCE for 2000 s: (a,b) SEM image of electrodeposited sample at low and high magnification; (c,d) SEM image of sample calcined at 900 °C for 12 h at low and high magnification; (e) nano-XRF/XRF distribution; (f) stability test in the catalytic partial oxidation of CH₄ at different reaction conditions; and (g) HR-TEM image of spent catalyst. Adapted from [60].

In other words, the control of the composition of Rh/Mg/Al HT coatings was of paramount importance for the preparation of the structured catalysts with enhanced properties in terms of stability of the catalytic coating and of the active sites dispersed on it. The use of a flow cell double-compartment set-up was the key to achieve this. A short overview of the properties of a typical case—Rh/Mg/Al HT electrodeposited on the FeCrAl foam—is displayed in Figure 9. With the same electrolyte, Rh/Mg/Al = 5/70/25 (a.r.%), the flow cell allowed to control better the composition of the solid deposited and therefore the catalysts properties and catalytic activity, likewise for conventional coprecipitated catalysts.

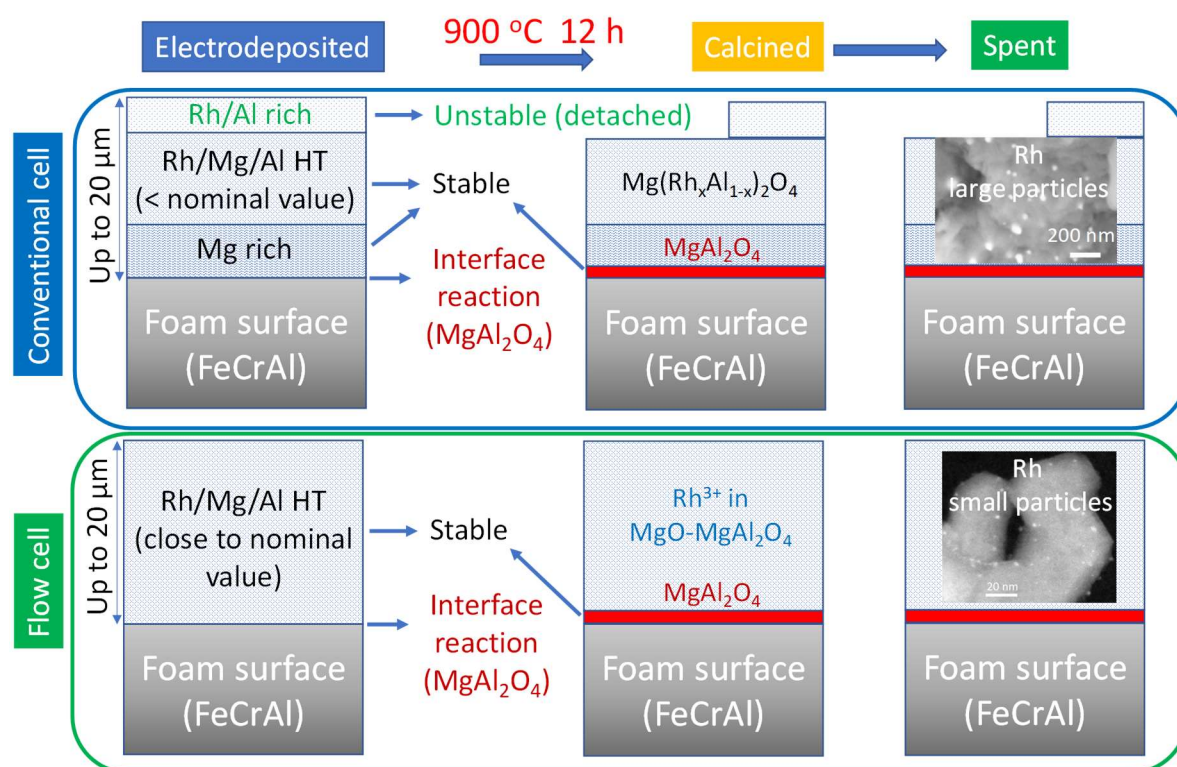


Figure 9. Model of Rh/Mg/Al HT layers electrodeposited on FeCrAl foam in a conventional cell (single compartment) and a flow cell (double-compartment) through the life-time of the catalysts from electrodeposition to the spent state after using for the CPO of CH₄.

4. Conclusions

The electro-base generation method is a promising route to in situ coat open-cell metallic foams with HT compounds, obtaining, after calcination, structured catalysts for syngas production processes by SR and CPO of CH₄. The electro- and chemical processes taking place at the electrode-electrolyte interface are determined not only by the potential applied and time, but also by the composition of the electrolyte and the set-up. The potential applied controls the electrochemical reactions, mainly nitrate reduction with some contribution of water electrolysis; while, the presence of precipitating cations catalyze the reduction processes. The composition of the electrolyte must be carefully tailored considering that: (i) the reduction of Rh³⁺ may be avoided by adjusting the initial pH; (ii) the KNO₃ supporting electrolyte must be removed to prevent K contamination; (iii) the modification of the total metal concentration determines the amount of solid deposited, composition and crystalline phases. Since the structured catalysts are obtained by calcination at high temperature, i.e., 900 °C, their properties also depend on the chemical/mechanical processes occurring during calcination. The composition and crystalline phases of thin Ni/Al coatings may be easily controlled; thus, the final catalysts achieve good performances in the SR. On the other hand, in the case of thick Rh/Mg/Al films the replenishment of the solution and the separation of working and counter electrode seems to be of paramount importance. Under optimized conditions coprecipitated-like coatings with a MgAl₂O₄ layer in the coating/foam interface, due to the coating-support interaction, were obtained, and the structured catalysts showed high activity and stability for the CPO of CH₄.

Author Contributions: P.H.H. performed the experiments in Sections 2 and 3.2.3; he also contributed to writing the article. E.S. and D.T. contributed to the design of electrodepositions, discussion of the results and writing the article. G.F. and A.V. contributed to the discussion of the catalytic data and writing the article. P.B. supervised the work, she contributed to the design of the electrodepositions, catalytic tests and characterizations, she contributed to write the article.

Funding: P.H.H. thanks to SINCHEM grant for Ph.D. research fellowship. SINCHEM is a joint-doctorate programme selected under Erasmus Mundus Action 1 programme (FBA 2013-0037).

Conflicts of Interest: The authors declare no conflict of interest.

References

1. Tronconi, E.; Groppi, G.; Visconti, C.G. Structured catalysts for non-adiabatic applications. *Curr. Opin. Chem. Eng.* **2014**, *5*, 55–67. [[CrossRef](#)]
2. Montebelli, A.; Visconti, C.G.; Groppi, G.; Tronconi, E.; Cristiani, C.; Ferreira, C.; Kohler, S. Methods for the catalytic activation of metallic structured substrates. *Catal. Sci. Technol.* **2014**, *4*, 2846–2870. [[CrossRef](#)]
3. Bianchi, E.; Heidig, T.; Visconti, C.G.; Groppi, G.; Freund, H.; Tronconi, E. An appraisal of the heat transfer properties of metallic open-cell foams for strongly exo-/endo-thermic catalytic processes in tubular reactors. *Chem. Eng. J.* **2012**, *198–199*, 512–528. [[CrossRef](#)]
4. Bianchi, E.; Heidig, T.; Visconti, C.G.; Groppi, G.; Freund, H.; Tronconi, E. Heat transfer properties of metal foam supports for structured catalysts: Wall heat transfer coefficient. *Catal. Today* **2013**, *216*, 121–134. [[CrossRef](#)]
5. Klumpp, M.; Inayat, A.; Schwerdtfeger, J.; Körner, C.; Singer, R.F.; Freund, H.; Schwieger, W. Periodic open cellular structures with ideal cubic cell geometry: Effect of porosity and cell orientation on pressure drop behavior. *Chem. Eng. J.* **2014**, *242*, 364–378. [[CrossRef](#)]
6. Inayat, A.; Klumpp, M.; Lämmermann, M.; Freund, H.; Schwieger, W. Development of a new pressure drop correlation for open-cell foams based completely on theoretical grounds: Taking into account strut shape and geometric tortuosity. *Chem. Eng. J.* **2016**, *287*, 704–719. [[CrossRef](#)]
7. Giani, L.; Cristiani, C.; Groppi, G.; Tronconi, E. Washcoating method for Pd/ γ -Al₂O₃ deposition on metallic foams. *Appl. Catal. B Environ.* **2006**, *62*, 121–131. [[CrossRef](#)]
8. Cristiani, C.; Finocchio, E.; Latorrata, S.; Visconti, C.G.; Bianchi, E.; Tronconi, E.; Groppi, G.; Pollesel, P. Activation of metallic open-cell foams via washcoat deposition of Ni/MgAl₂O₄ catalysts for steam reforming reaction. *Catal. Today* **2012**, *197*, 256–264. [[CrossRef](#)]
9. Montebelli, A.; Visconti, C.G.; Groppi, G.; Tronconi, E.; Kohler, S.; Venvik, H.J.; Myrstad, R. Washcoating and chemical testing of a commercial Cu/ZnO/Al₂O₃ catalyst for the methanol synthesis over copper open-cell foams. *Appl. Catal. A Gen.* **2014**, *481*, 96–103. [[CrossRef](#)]
10. Balzarotti, R.; Cristiani, C.; Francisc, L.F. Spin coating deposition on complex geometry substrates: Influence of operative parameters. *Surf. Coat. Technol.* **2017**, *330*, 1–9. [[CrossRef](#)]
11. Bortolozzi, J.P.; Weiss, T.; Gutierrez, L.B.; Ulla, M.A. Comparison of Ni and Ni–Ce/Al₂O₃ catalysts in granulated and structured forms: Their possible use in the oxidative dehydrogenation of ethane reaction. *Chem. Eng. J.* **2014**, *246*, 343–352. [[CrossRef](#)]
12. Banús, E.D.; Ulla, M.A.; Miró, E.E.; Milt, V.G. Co,Ba,K/ZrO₂ coated onto metallic foam (AISI 314) as a structured catalyst for soot combustion: Catalytic activity and stability. *Appl. Catal. A Gen.* **2011**, *393*, 9–16. [[CrossRef](#)]
13. Yang, H.; Li, J.; Yu, H.; Peng, F.; Wang, H. Metal-Foam-Supported Pd/Al₂O₃ Catalysts for Catalytic Combustion of Methane: Effect of Interaction between Support and Catalyst. *Int. J. Chem. React. Eng.* **2015**, *13*, 83–93. [[CrossRef](#)]
14. Liu, Y.; Xu, J.; Li, H.; Cai, S.; Hu, H.; Fang, C.; Shi, L.; Zhang, D. Rational design and in situ fabrication of MnO₂@NiCo₂O₄ nanowire arrays on Ni foam as high-performance monolith de-NO_x catalysts. *J. Mater. Chem. A* **2015**, *3*, 11543–11553. [[CrossRef](#)]
15. Fang, C.; Shi, L.; Hu, H.; Zhang, J.; Zhang, D. Rational design of 3D hierarchical foam-like Fe₂O₃@CuO_x monolith catalysts for selective catalytic reduction of NO with NH₃. *RSC Adv.* **2015**, *5*, 11013–11022. [[CrossRef](#)]
16. Kryca, J.; Jodłowski, P.J.; Iwaniszyn, M.; Gil, B.; Sitarz, M.; Kołodziej, A.; Łojewska, T.; Łojewska, J. Cu SSZ-13 zeolite catalyst on metallic foam support for SCR of NO_x with ammonia: Catalyst layering and characterisation of active sites. *Catal. Today* **2016**, *268*, 142–149. [[CrossRef](#)]
17. Liang, Z.; Gao, P.; Tang, Z.; Lv, M.; Sun, Y. Three dimensional porous Cu–Zn/Al foam monolithic catalyst for CO₂ hydrogenation to methanol in microreactor. *J. CO₂ Utiliz.* **2017**, *21*, 191–199. [[CrossRef](#)]

18. Freya, M.; Romero, T.; Roger, A.-C.; Edouard, D. Open cell foam catalysts for CO₂ methanation: Presentation of coating procedures and in situ exothermicity reaction study by infrared thermography. *Catal. Today* **2016**, *273*, 83–90. [[CrossRef](#)]
19. Méndez, F.J.; Sanz, O.; Montes, M.; Guerra, J.; Olivera-Fuentes, C.; Curbelo, S.; Brito, J.L. Selective hydrogenation of 1,3-butadiene in the presence of 1-butene under liquid phase conditions using structured catalysts. *Catal. Today* **2017**, *289*, 151–161. [[CrossRef](#)]
20. Chai, R.; Li, Y.; Zhang, Q.; Fan, S.; Zhang, Z.; Chen, P.; Zhao, G.; Liu, Y.; Lu, Y. Foam-Structured NiO–MgO–Al₂O₃ Nanocomposites Derived from NiMgAl Layered Double Hydroxides In Situ Grown onto Nickel Foam: A Promising Catalyst for High-Throughput Catalytic Oxymethane Reforming. *ChemCatChem* **2017**, *9*, 268–272. [[CrossRef](#)]
21. Cao, C.; Xing, L.; Yang, Y.; Tian, Y.; Ding, T.; Zhang, J.; Hu, T.; Zheng, L.; Li, X. The monolithic transition metal oxide crossed nanosheets used for diesel soot combustion under gravitational contact mode. *Appl. Surf. Sci.* **2017**, *406*, 245–253. [[CrossRef](#)]
22. Therese, G.H.A.; Kamath, P.V. Electrochemical Synthesis of Metal Oxides and Hydroxides. *Chem. Mater.* **2000**, *12*, 1195–1204. [[CrossRef](#)]
23. Cattarin, S.; Musiani, M. Electrosynthesis of nanocomposite materials for electrocatalysis. *Electrochim. Acta* **2007**, *52*, 2796–2805. [[CrossRef](#)]
24. Bicelli, L.P.; Bozzini, B.; Mele, C.; D’Urzo, L. A Review of Nanostructural Aspects of Metal Electrodeposition. *Int. J. Electrochem. Sci.* **2008**, *3*, 356–408.
25. Chandrasekar, M.S.; Pushpavanam, M. Pulse and pulse reverse plating—Conceptual, advantages and applications. *Electrochim. Acta* **2008**, *53*, 3313–3322. [[CrossRef](#)]
26. Gurrappa, I.; Binder, L. Electrodeposition of nanostructured coatings and their characterization—A Review. *Sci. Technol. Adv. Mater.* **2008**, *9*, 043001. [[CrossRef](#)] [[PubMed](#)]
27. Choi, K.-S.; Jang, H.S.; McShane, C.M.; Read, C.G.; Seabold, J.A. Electrochemical Synthesis of Inorganic Polycrystalline Electrodes with Controlled Architectures. *MRS Bull.* **2010**, *35*, 753–760. [[CrossRef](#)]
28. Wu, X.-J.; Zhu, F.; Mu, C.; Liang, Y.; Xu, L.; Chen, Q.; Chen, R.; Xu, D. Electrochemical synthesis and applications of oriented and hierarchically quasi-1D semiconducting nanostructures. *Coord. Chem. Rev.* **2010**, *254*, 1135–1150. [[CrossRef](#)]
29. Mohanty, U.S. (Ed.) *Electrodeposition: Properties, Processes and Applications*; Nova Science Publishers: Hauppauge, NY, USA, 2012.
30. Kang, D.; Kim, T.W.; Kubota, S.R.; Cardiel, A.C.; Cha, H.G.; Choi, K.-S. Electrochemical Synthesis of Photoelectrodes and Catalysts for Use in Solar Water Splitting. *Chem. Rev.* **2015**, *115*, 12839–12887. [[CrossRef](#)] [[PubMed](#)]
31. Ustarroz, J.; Hubin, A.; Terryn, H. *Supported Nanoparticle Synthesis by Electrochemical Deposition in Handbook of Nanoparticles*; Aliofkhaezrai, M., Ed.; Springer International Publishing: Basel, Switzerland, 2016; pp. 603–631.
32. Roger, I.; Symes, M.D. First row transition metal catalysts for solar-driven water oxidation produced by electrodeposition. *J. Mater. Chem. A* **2016**, *4*, 6724–6741. [[CrossRef](#)]
33. Ng, P.K.; Schneider, E.W. Distribution of Nickel Hydroxide in Sintered Nickel Plaques Measured by Radiotracer Method during Electroimpregnation. *J. Electrochem. Soc.* **1986**, *133*, 17–21. [[CrossRef](#)]
34. Ho, K.C. Electrochemical Precipitation of Nickel Hydroxide. *J. Electrochem. Soc.* **1987**, *134*, 52C–55C. [[CrossRef](#)]
35. Indira, L.; Kamath, P.V. Electrogenation of base by cathodic reduction of anions: Novel one-step route to unary and layered double hydroxides (LDHs). *J. Mater. Chem.* **1994**, *4*, 1487–1490. [[CrossRef](#)]
36. Dixit, M.; Kamath, P.V. Electrosynthesis and stabilization of α -cobalt hydroxide in the presence of trivalent cations. *J. Power Sources* **1995**, *56*, 97–100. [[CrossRef](#)]
37. Tonelli, D.; Scavetta, E.; Giorgetti, M. Layered-double-hydroxide-modified electrodes: Electroanalytical applications. *Anal. Bioanal. Chem.* **2013**, *405*, 603–614. [[CrossRef](#)] [[PubMed](#)]
38. Shao, M.; Zhang, R.; Li, Z.; Wei, M.; Evans, D.G.; Duan, X. Layered double hydroxides toward electrochemical energy storage and conversion: Design, synthesis and applications. *Chem. Commun.* **2015**, *51*, 15880–15893. [[CrossRef](#)] [[PubMed](#)]
39. Vlamidis, Y.; Scavetta, E.; Giorgetti, M.; Sangiorgi, N.; Tonelli, D. Electrochemically synthesized cobalt redox active layered double hydroxides for supercapacitors development. *Appl. Clay Sci.* **2017**, *143*, 151–158. [[CrossRef](#)]

40. Li, Y.; Zhang, L.; Xiang, X.; Yan, D.; Li, F. Engineering of ZnCo-layered double hydroxide nanowalls toward high-efficiency electrochemical water oxidation. *J. Mater. Chem. A* **2014**, *2*, 13250–13258. [[CrossRef](#)]
41. Burke, M.S.; Kast, M.G.; Trotochaud, L.; Smith, A.M.; Boettcher, S.W. Cobalt–Iron (Oxy)hydroxide Oxygen Evolution Electrocatalysts: The Role of Structure and Composition on Activity, Stability, and Mechanism. *J. Am. Chem. Soc.* **2015**, *137*, 3638–3648. [[CrossRef](#)] [[PubMed](#)]
42. Vlamidis, Y.; Scavetta, E.; Gazzano, M.; Tonelli, D. Iron vs Aluminum Based Layered Double Hydroxides as Water Splitting Catalysts. *Electrochim. Acta* **2016**, *188*, 653–660. [[CrossRef](#)]
43. Liu, Y.; Fu, N.; Zhang, G.; Xu, M.; Lu, W.; Zhou, L.; Huan, H. Design of Hierarchical Ni-Co@Ni-Co Layered Double Hydroxide Core–Shell Structured Nanotube Array for High-Performance Flexible All-Solid-State Battery-Type Supercapacitors. *Adv. Funct. Mater.* **2017**, *27*, 1605307. [[CrossRef](#)]
44. Jagadale, A.D.; Guan, G.; Li, X.; Du, X.; Ma, X.; Hao, X.; Abudula, A. Binder-Free Electrodes of CoAl Layered Double Hydroxide on Carbon Fibers for All-Solid-State Flexible Yarn Supercapacitors. *Energy Technol.* **2016**, *4*, 997–1004. [[CrossRef](#)]
45. Li, H.; Musharavati, F.; Zalenezhad, E.; Chen, X.; Hui, K.N.; Hui, K.S. Electrodeposited Ni-Co layered double hydroxides on titanium carbide as a binder-free electrode for supercapacitors. *Electrochim. Acta* **2018**, *261*, 178–187. [[CrossRef](#)]
46. Liu, Y.; Teng, X.; Mi, Y.; Chen, Z. A new architecture design of Ni-Co LDH-based Pseudocapacitors. *J. Mater. Chem. A* **2017**, *5*, 24407–24415. [[CrossRef](#)]
47. Bo, X.; Li, Y.; Hocking, R.K.; Zhao, C. NiFeCr Hydroxide Holey Nanosheet as Advanced Electrocatalyst for Water Oxidation. *ACS Appl. Mater. Interfaces* **2017**, *9*, 41239–41245. [[CrossRef](#)] [[PubMed](#)]
48. Basile, F.; Benito, P.; Del Gallo, P.; Fornasari, G.; Gary, D.; Rosetti, V.; Scavetta, E.; Tonelli, D.; Vaccari, A. Highly conductive Ni steam reforming catalysts prepared by electrodeposition. *Chem. Commun.* **2008**, 2917–2919, 2917–2919. [[CrossRef](#)] [[PubMed](#)]
49. Verlato, E.; Barison, S.; Cimino, S.; Dergal, F.; Lisi, L.; Mancino, G.; Musiani, M.; Vazquez-Gómez, L. Catalytic partial oxidation of methane over nanosized Rh supported on FeCrAlloy foams. *Int. J. Hydrogen Energy* **2014**, *39*, 11473–11485. [[CrossRef](#)]
50. Cimino, S.; Gambirasi, A.; Lisi, L.; Mancino, G.; Musiani, M.; Vázquez-Gómez, L.; Verlato, E. Catalytic combustion of methanol on Pt–FeCrAlloy foams prepared by electrodeposition. *Chem. Eng. J.* **2016**, *285*, 276–285. [[CrossRef](#)]
51. Verlato, E.; Barison, S.; Cimino, S.; Lisi, L.; Mancino, G.; Musiani, M.; Paolucci, F. Electrochemical preparation of nanostructured CeO₂-Pt catalysts on Fe-Cr-Al alloy foams for the low-temperature combustion of methanol. *Chem. Eng. J.* **2017**, *317*, 551–560. [[CrossRef](#)]
52. Cavani, F.; Trifirò, F.; Vaccari, A. Hydrotalcite-type anionic clays: Preparation, properties and applications. *Catal. Today* **1991**, *11*, 173–301. [[CrossRef](#)]
53. Ho, P.H.; Monti, M.; Scavetta, E.; Tonelli, D.; Bernardi, E.; Nobili, L.; Fornasari, G.; Vaccari, A.; Benito, P. Reactions involved in the electrodeposition of hydrotalcite-type compounds on FeCrAlloy foams and plates. *Electrochim. Acta* **2016**, *222*, 1335–1344. [[CrossRef](#)]
54. Milhano, C.; Pletcher, D. The Electrochemistry and Electrochemical Technology of Nitrate. In *Modern Aspects of Electrochemistry*, No. 45; White, R.E., Ed.; Springer: New York, NY, USA, 2009; pp. 1–61.
55. Ho, P.H.; Scavetta, E.; Ospitali, F.; Tonelli, D.; Fornasari, G.; Vaccari, A.; Benito, P. Effect of metal nitrate concentration on the electrodeposition of hydrotalcite-like compounds on open-cell foams. *Appl. Clay Sci.* **2018**, *151*, 109–117. [[CrossRef](#)]
56. Basile, F.; Benito, P.; Fornasari, G.; Vaccari, A. Hydrotalcite-type precursors of active catalysts for hydrogen production. *Appl. Clay Sci.* **2010**, *48*, 250–259. [[CrossRef](#)]
57. Monti, M.; Benito, P.; Basile, F.; Fornasari, G.; Gazzano, M.; Scavetta, E.; Tonelli, D.; Vaccari, A. Electrosynthesis of Ni/Al and Mg/Al Layered Double Hydroxides on Pt and FeCrAlloy supports: Study and control of the pH near the electrode surface. *Electrochim. Acta* **2013**, *108*, 596–604. [[CrossRef](#)]
58. Benito, P.; Monti, M.; Bersani, I.; Basile, F.; Fornasari, G.; Scavetta, E.; Tonelli, D.; Vaccari, A. Coating of FeCrAlloy foam with Rh catalysts: Optimization of electrosynthesis parameters and catalyst composition. *Catal. Today* **2012**, *197*, 162–169. [[CrossRef](#)]
59. Benito, P.; Monti, M.; De Nolf, W.; Nuyts, G.; Janssen, G.; Fornasari, G.; Scavetta, E.; Basile, F.; Janssens, K.; Ospitali, F.; et al. Improvement in the coating homogeneity in electrosynthesized Rh structured catalysts for the partial oxidation of methane. *Catal. Today* **2015**, *246*, 154–164. [[CrossRef](#)]

60. Ho, P.H.; de Nolf, W.; Ospitali, F.; Gondolini, A.; Fornasari, G.; Scavetta, E.; Tonelli, D.; Vaccari, A.; Benito, P. Coprecipitated-like hydrotalcite-derived coatings on open-cell metallic foams by electrodeposition: Rh nanoparticles on oxide layers stable under harsh reaction conditions. *Appl. Catal. A Gen.* **2018**, *560*, 12–20. [[CrossRef](#)]
61. Basile, F.; Benito, P.; Fornasari, G.; Monti, M.; Scavetta, E.; Tonelli, D.; Vaccari, A. Novel Rh-based structured catalysts for the catalytic partial oxidation of methane. *Catal. Today* **2010**, *157*, 183–190. [[CrossRef](#)]
62. Basile, F.; Benito, P.; Fornasari, G.; Rosetti, V.; Scavetta, E.; Tonelli, D.; Vaccari, A. Electrochemical synthesis of novel structured catalysts for H₂ production. *Appl. Catal. B Environ.* **2009**, *91*, 563–572. [[CrossRef](#)]
63. Benito, P.; Nuyts, G.; Monti, M.; De Nolf, W.; Fornasari, G.; Janssens, K.; Scavetta, E.; Vaccari, A. Stable Rh particles in hydrotalcite-derived catalysts coated on FeCrAlloy foams by electrosynthesis. *Appl. Catal. B Environ.* **2015**, *179*, 321–332. [[CrossRef](#)]
64. Benito, P.; de Nolf, W.; Nuyts, G.; Monti, M.; Fornasari, G.; Basile, F.; Janssens, K.; Ospitali, F.; Scavetta, E.; Tonelli, D.; et al. Role of Coating-Metallic Support Interaction in the Properties of Electrosynthesized Rh-Based Structured Catalysts. *ACS Catal.* **2014**, *4*, 3779–3790. [[CrossRef](#)]
65. Scavetta, E.; Mignani, A.; Prandstraller, D.; Tonelli, D. Electrosynthesis of Thin Films of Ni, Al Hydrotalcite Like Compounds. *Chem. Mater.* **2007**, *19*, 4523–4529. [[CrossRef](#)]
66. Basile, F.; Benito, P.; Bugani, S.; De Nolf, W.; Fornasari, G.; Janssens, K.; Morselli, L.; Scavetta, E.; Tonelli, D.; Vaccari, A. Combined Use of Synchrotron-Radiation-Based Imaging Techniques for the Characterization of Structured Catalysts. *Adv. Funct. Mater.* **2010**, *20*, 4117–4126. [[CrossRef](#)]
67. Bard, A.J.; Faulkner, L.R. *Electrochemical methods: Fundamentals and Applications*, 2nd ed.; John Wiley & Sons: New York, NY, USA, 2000.



© 2018 by the authors. Licensee MDPI, Basel, Switzerland. This article is an open access article distributed under the terms and conditions of the Creative Commons Attribution (CC BY) license (<http://creativecommons.org/licenses/by/4.0/>).